Original article

Pterostilbene induces apoptosis in hepatocellular carcinoma cells: Biochemical, pathological, and molecular markers

Mahmoud I. Khalil [a,b,*], Alaa F. Agamy [b], Salma S. Elshewemi [c], Ahmed S. Sultan [d], Nabila E. Abdelmeguid [c]

[a] Department of Biological Sciences, Faculty of Science, Beirut Arab University, Lebanon
[b] Molecular Biology Unit, Zoology Department, Faculty of Science, Alexandria University, Egypt
[c] Zoology Department, Faculty of Science, Alexandria University, Egypt
[d] Biochemistry Department, Faculty of Science, Alexandria University, Egypt

ARTICLE INFO

ABSTRACT

Worldwide, hepatocellular carcinoma (HCC) is considered the sixth most prevalent cancer and ranked third in causes leading to death. Pterostilbene (PTE), a dimethylated analog of resveratrol, is a phytochemical found in fruits such as blueberries and grapes, and is known for its anticancer effect. The current study intended to investigate the effect of PTE on HepG2 cells. Cell viability, colony-forming potential, lipid peroxidation, catalase enzyme (CAT), superoxide dismutase (SOD), and caspase 3 activities, histone release, and expression levels of mTOR, S6K1, p53, and STAT3 proteins were assessed in PTE-treated HepG2 cells. In addition, the cellular and ultrastructural alterations were evaluated by light and transmission electron microscopy. PTE induced a significant reduction in HepG2 viability in a dose-dependent manner (IC$_{50}$ of PTE = 74 ± 6 μM), accompanied by a decrease in colony formation potential. PTE-treated cancer cells exhibited a decrease in lipid peroxidation and CAT activity, and an increase in histone release, caspase-3, and SOD activities. Ultrastructurally, PTE-treated cells exhibited notable cell shrinkage, reduced number of filopodia, increased vacuolization, apoptotic bodies, accumulation of lipid droplets, enlarged mitochondria, dilated endoplasmic reticulum, pyknotic nuclei, and cellular fragmentation. mTOR, S6K1, and STAT3 levels were downregulated, however p53 level was modulated in PTE-treated cells. The anticancer potential of PTE might be related to its ability to alter the ultrastructure morphology, reduce mitotic activity, and modulate some key protein required for cell proliferation, suggesting its potential to trigger cancer cells towards apoptosis.

© 2023 The Author(s). Published by Elsevier B.V. on behalf of King Saud University. This is an open access article under the CC BY-NC-ND license (http://creativecommons.org/licenses/by-nc-nd/4.0/).

1. Introduction

Cancer is expected to spread further and increase in its incidence in the coming century (Siegel et al., 2020). Cancer is characterized by a notable malfunction in the balance machinery between cell division and cell death (Singh et al., 2019). Hepatocellular carcinoma (HCC) is considered the sixth most prevalent cancer and is more likely to occur in men (Sung et al., 2021). The risk factors for HCC can be divided into infectious risk factors such as hepatitis B and C viruses (HBV and HCV), and non-infectious risk factors such as smoking, alcohol, and exposure to chemical compounds. Moreover, there are host-related risk factors such as gender, ethnicity, diet, oral contraceptives, diabetes, and the genetic background of the host (Rashed et al., 2020). Middle- and low-income countries have high rates of HCC. HCC is more abundant in regions with endemic HBV and HCV infections (Petruzziello, 2018).

Stilbenes are phenolic compounds found naturally in various plants. Stilbenes are synthesized in plants through the phenylpropanoid pathway, a mechanism similar to that of flavonoid synthesis (Akinwumi et al., 2018). Pterostilbene (PTE) (*trans*-3, 5-dimethoxy-4- hydroxystilbene) is a phytochemical stilbene found in grapes and blueberries (McCormack and McFadden, 2013). It is a dimethylated analogue of resveratrol, a well-known antioxidant, which has anticancer activity, but with more bioavailability. Due to its structure similar to that of resveratrol, PTE has significant

* Corresponding author at: Department of Biological Sciences, Faculty of Science, Beirut Arab University, Lebanon. Molecular Biology Unit, Zoology Department, Faculty of Science, Alexandria University, Egypt.

E-mail addresses: mahmoud_ibrahim@alexu.edu.eg, m.khalil@bau.edu.lb (M.I. Khalil), alaa.agamy_pg@alexu.edu.eg (A.F. Agamy), salma.elshewemi@alexu.edu.eg (S.S. Elshewemi), drasultan@alexu.edu.eg (A.S. Sultan), nabila.elsayed@alexu.edu.eg (N.E. Abdelmeguid).

Peer review under responsibility of King Saud University.

antioxidant and anticancer activities (Akinwumi et al., 2018). Furthermore, PTE has been proven to significantly inhibit the growth, adhesion, and metastatic potential of different cancers (Elsherbini et al., 2020; Remsberg et al., 2008).

Apoptosis is a normal physiological process committed by the damaged cells under a tightly controlled system to eliminate the abnormal cells from the cellular population (Singh et al., 2019). A variety of intracellular stress can trigger apoptosis such as oxidative stress, DNA damage, deficiency of growth factors, exposure to toxins, reactive oxygen species (ROS) overload, and endoplasmic reticulum (ER) stress (Checa and Aran, 2020). Regardless of the nature of the initiating stimulus of apoptosis or the intracellular organelle from which it originates, all lead to intracellular signaling cascades that result in mitochondrial dysfunction and mitochondrial outer membrane permeabilization (MOMP) (Singh et al., 2019). MOMP causes the release of cytochrome c in the cytoplasm and forms an apoptosome with the APAF1, the apoptotic protease activating factor 1 (Cavalcante et al., 2019). This complex hydrolyses ATP and upregulates the activation of caspase-9 which in turn cleaves/activates caspase-3, -6, and -7 (Zhu et al., 2012). As a result, caspase-3 promotes DNA fragmentation which is followed by apoptosis (Cavalcante et al., 2019).

There are a number of morphological and biochemical features that are unique to apoptosis including, disturbance in the antioxidant enzymes, notable shrinkage in the cell's size, blebbing of the cell membrane, chromatin condensation, fragmentation of DNA, and development of apoptotic bodies, followed by engulfing of dying cells by macrophage-mediated phagocytosis (Elmore, 2007). Metastasis, a hallmark of malignancy, is mainly dependent on the migration and invasive ability of cancer cells (Tahtamouni et al., 2019). Migration of cancer cells is a complicated process controlled by many factors including the dynamics of the cytoskeleton and filopodia, which are finger-shaped cell protrusions formed of bundled actin, as well as alterations in the molecular expression of some adhesion and proteolytic enzymes (Gallop, 2020).

p53 is a key tumour suppressor protein that serves as a sensor of cellular stress and responds to various stress signals either by inducing apoptosis or cell cycle arrest (Cui et al., 2021). The mammalian target of rapamycin (mTOR) pathway is a key regulator of a variety of cellular activities including; cell metabolism, proliferation, growth, and survival (Zou et al., 2020). mTOR pathway is upregulated in different cancers, angiogenesis, insulin resistance, adipogenesis, and T-lymphocyte activation (Feng et al., 2021; Ferrín et al., 2020; Khalil and Gout, 2012). The current study aimed to investigate the effect of PTE on hepatocellular carcinoma cells, HepG2. Key proteins involved in cell proliferation and growth were assessed, including mTOR, S6K1, p53, and STAT3 proteins. In addition, cellular and ultrastructural alterations were investigated by light and transmission electron microscopy.

2. Materials and methods

2.1. Cell culture

HepG2 cells (ATCC, USA) were cultured/passaged in DMEM (Dulbecco modified Eagle Minimum Essential Medium), supplemented with 10% fetal bovine serum (FBS), and 50 IU/ml penicillin/streptomycin. Cancer cells were cultured in 25 cm^3 tissue flasks at 37 °C in an incubator with 5% CO_2.

2.2. Cell viability assay

The MTT cell viability assay was performed using the Cell Proliferation Assay Kit (Invitrogen). Briefly, 96-well plates were used to seed 10^5 cells/mL in complete DMEM. Cancer cells were treated

24 h later with 10–150 μM PTE (P1499-10MG; Sigma-Aldrich, USA). After 48 hrs, the medium was replaced with a fresh medium supplemented with 12 mM MTT (3-(4,5-dimethylthiazol-2-yl)-2,5-diphenyltetrazolium bromide) to each well. Cells were further incubated for 4 hrs at 37 °C. 100 μl of SDS-HCl solution was added to each well. The 96-well plate was incubated in a humidified chamber at 37 °C for 18 h. The results of three independent experiments were normalizing to their respective controls and represented as mean ± SEM. The absorbance (A) was measured at 545 nm using an ELISA microplate reader (ELISA Unit. Stat Fax 2100, USA). The cell viability percentage (%) was calculated as follows:

$$\text{Cell viability}\,(\%) = \frac{A_{sample} - A_{blank}}{A_{control} - A_{blank}} \times 100$$

The inhibitory concentration of PTE that resulted in the inhibition of 50% cell viability (IC$_{50}$ PTE) was determined from the trendline of a sigmoidal curve that shows the effect of PTE (represented by the log concentrations of PTE) on the cell viability percentage of HepG2 cells.

2.3. Clonogenic assay

6×10^3 HepG2 cells were seeded per well in a 12-well plate prior to treatment with different concentrations of PTE. Untreated cells were used as a control. After 48 hrs, the culture medium was replaced with a fresh medium with no PTE. After two weeks, colonies were fixed with absolute methanol for 20 min before staining with 2% crystal violet for 3 min. Digital images of the colonies were obtained using Kodac digital camera (Kodak, USA), and colony areas were calculated using ImageJ software (NIH, USA).

2.4. Biochemical assays

In a complete DMEM, 3.5×10^6 HepG2 cells were seeded prior to PTE treatment. Cells were rinsed in ice-cold PBS prior to lysis in lysis buffer (10 mM HEPES pH 7.4, 2 mM EDTA, 0.1% CHAPS, 350lg/ml PMSF and 5 mM DTT). The cells were spun at 15000 rpm (4 °C) for 15 min. The cleared lysates were used to assess lipid peroxidation (Malondialdehyde; MDA (mol/ml)), catalase (CAT (U/ml)), and superoxide dismutase (SOD (U/ml)) activities following the instructions provided with the corresponding assay kit (Bio-Diagnostic,Egypt). Caspase-3 activity (U/ml) was evaluated using the Colorimetric kit (Bio Vision, Inc., CA, USA). The absorbances were recorded using an ELISA microplate reader (ELISA Unit. Stat Fax 2100, USA) at 534 nm, 510 nm, 560 nm, and 405 nm, for the MDA, CAT, SOD, and Caspase-3 assays, respectively. The results of each assay were generated from three independent trials.

2.5. Apoptosis enzyme-linked immunosorbent assay

In a complete DMEM, 2×10^4 HepG2 cells were seeded and allowed to attach before treatment with PTE. Cells were washed in ice-cold PBS prior to lysis using ice-cold lysis buffer (10 mM HEPES pH 7.4, 2 mM EDTA, 0.1% CHAPS, 350lg/ml PMSF and 5 mM DTT) for 30 min on ice. Cell lysates were spun at 15000 rpm (4 °C) for 30 min. 20 μl of the supernatant was incubated at RT, with anti-histone biotin and anti-DNA peroxidase in a streptavidin-coated microplate for 2 hrs. Each well was subjected to 100 μl of substrate solution (ABTS (2,2′-azinodi-3 ethylbenzthiazolinesulfonic acid) and incubated at room temperature for additional 15–20 min. The absorbance was recorded using an ELISA microplate reader (ELISA Unit. Stat Fax 2100, USA).

2.6. Light (LM) and transmission electron microscopy (TEM)

Cultured HepG2 cells were harvested by centrifugation at 1000 rpm (4 °C) from 25 cm^3 tissue culture flasks after 48 h of PTE treatment. Semithin sections (1 μm thickness) were fixed in a Formalin-Glutaradehyde mixture ($_4F_1G$) (4% Formaldehyde & 1% Glutaraldehyde in 0.1 M PBS, pH7.4), then postfixed in 1% OsO$_4$, dehydrated in ethanol, then embedded in Epon and stained with 1% Toluidine Blue. Sections were examined with a LM and photographed. Morphometric measurements of HepG2 cells in light micrographs have been determined using ImageJ software (NIH, USA) and statistically analyzed. For the TEM, cultured HepG2 cells were collected by centrifugation at 1000 rpm (4 °C) from 25 cm^2 tissue culture flasks after 48 hrs of PTE treatment prior to immediate immersing in $_4F_1G$, and then rinsed for 2 hrs. in 0.1 M PBS at 4 °C. Post-fixation was carried out using 1% OsO$_4$ at 4 °C for 2 hrs. Samples were dehydrated through a graded series of ethanol, treated with propylene oxide, and inserted in an Araldite-Epon mixture. Ultrathin (70 nm) sections were cut using a glass-knife on LKB-ultra-tome and were picked on 200 mesh-naked copper grids. Following double-staining with lead citrate and uranyl acetate, sections were assessed under Jeol 100 CX Electron Microscope (TESCAN, USA) at 80 kV. Ultrastructural changes/ observations of untreated or PTE-treated HepG2 cells were assessed on a scale from (−) to (+++) as follows: (−) = no change, (+) = mild change, (++) = moderate change, and (+++) = severe change (Elsawy et al., 2021; Suzuki and Suzuki, 1998). Parameters that were investigated include apoptotic body, pyknotic nuclei, mitotic figure, pleomorphic mitochondria, aggregated mitochondria, enlarged mitochondria, dilated endoplasmic reticulum, filopodia, vacuolated cytoplasm, and cellular junction. A minimum of three sections per sample were examined by a pathologist.

2.7. Immunoblotting

In a complete DMEM, HepG2 cells were seeded and then treated with PTE. Cells were washed in ice-cold PBS prior to lysis in ice-cold lysis buffer (10 mM HEPES pH7.4, 2 mM EDTA, 0.1% CHAPS, 350lg/ml PMSF and 5 mM DTT). The cells were centrifuged at 15000 rpm (4 °C) for 15 min. After cell lysis, the cleared lysates were subjected to the Pierce BCA Assay Kit for protein concentration determination (Sigma Aldrich, USA). 30 μg of cleared lysates were run in 10% SDS-PAGE (90 min, 90–120 V). Gel was blotted onto a prewetted nitrocellulose membrane in transfer buffer (48 mM Tris base, 390 mM Glycine, 0.1%(w/v) SDS, 20% Methanol) (70 V − 2 h). The membranes were blocked for 30 min in blocking buffer (3%BSA solution in TBST) prior to the incubation with the primary antibody at the recommended dilution in blocking buffer [mTOR polyclonal antibody (1:1000), S6K1 polyclonal antibody (1: 1000)] (SantaCruz Biotech, USA). The membranes were washed in TBST for several times before incubation with the secondary antibody (1:10000 in TBST) at room temperature for 2 hrs. To assess protein expression levels, the TMB kit (Sigma-Aldrich, USA) was used. Band densitometry was quantified using Quantity One (BioRad, USA).

2.8. Statistical analysis

Data were represented as mean ± SEM. Student's *t-test* or one-way analysis of variance (ANOVA) was employed to compare between data. This was followed by Tukey's test using GraphPad Prism software (California, USA). For the cell viability assay, each calculated cell viability percentage at each PTE concentration used for treatments was compared with the untreated control cells and statistically evaluated using Student's *t-test*. Differences in results at $p < 0.05$ were considered as statistically significant.

3. Results

3.1. PTE reduces cell viability and colony-forming potential of HepG2 cells

The MTT assay revealed a dose-dependent inhibition in HepG2 cells proliferation upon treatment with increasing concentrations of PTE (10–150 μM). As shown in Fig. 1**a**, cell viability was significantly decreased upon treatment with 20 μM PTE. Highly significant deterioration in cell viability is exhibited upon PTE treatment with higher concentrations (80–150 μM). The calculated half-maximal growth inhibitory concentration (IC$_{50}$) of PTE was 74 ± 6 μM (Fig. 1**b**).

A colony-forming assay was employed to assess the ability of PTE to reduce the colony-forming potential of HepG2 cells. Cells were treated with ½IC$_{50}$ or IC$_{50}$ of PTE. The mean colony area, as well as the number of colonies, decreased with PTE treatment compared with untreated control cells (Fig. 1**c**).

3.2. PTE modulates oxidative stress and induces apoptosis in HepG2 cells

HepG2 cells treated with the IC$_{50}$ of PTE exhibited a significant reduction in malondialdehyde (MDA), a secondary product of lipid peroxidation, and catalase (CAT) activity. However, the treatment with IC$_{50}$ PTE resulted in an insignificant increase in the activity of superoxide dismutase (SOD) (Fig. 2**a**).

Caspase activity is a key apoptotic marker. Caspase-3 is essential for the apoptotic chromatin condensation and have a significant role in DNA fragmentation. Here, the treatments with the ½IC$_{50}$ or IC$_{50}$ of PTE led to a significant increase in the activity of caspase-3 in a dose-dependent manner (Fig. 2**b**). DNA fragmentation is an early event of apoptosis. The Apoptosis Enzyme-Linked Immunosorbent Assay helps in detecting the quantity of histones released in the cytoplasm which can reflect the extent of DNA fragmentation. Treatment with ½IC$_{50}$ or IC$_{50}$ PTE led to a significant increase in histone release, 193 % and 303 % increase, respectively, compared to untreated control cells (Fig. 2**c**).

3.3. PTE alters the morphology and reduces the mitotic activity of HepG2 cells

Semithin sections of the untreated HepG2 cells, treated with ½IC$_{50}$, or IC$_{50}$ of PTE were examined under light microscopy (Fig. 3). Examination of semi-thin sections of HepG2 cells showed that the cells exhibited two different morphologies, dark and light cells, according to the stainability of their nuclei and cytoplasm. Light cells possess less densely stained nuclei and lighter cytoplasm in comparison to these of the dark cells. The mitotic activity of the untreated cells was indicated by the presence of mitotic figures. Cells treated with ½IC$_{50}$ PTE exhibited some mitotic figures. However, no mitotic figures were detected in cells treated with IC$_{50}$ PTE. Features of apoptosis were observed after PTE treatment, including cellular and nuclear pleomorphism, cytoplasmic vacuolization, and increased incidence of pyknotic nuclei. Morphometric measurements of the light micrographs revealed a characteristic apoptotic feature which is the shrinkage of both light and dark cells after PTE treatment. PTE-treated cells showed a highly significant reduction in cellular and nuclear dimensions (Fig. 4).

3.4. PTE decreases the number of filopodia and induces ultrastructural alteration in HepG2 cells

To further investigate the subcellular alterations as a result of PTE treatment, control and PTE-treated cells were examined by
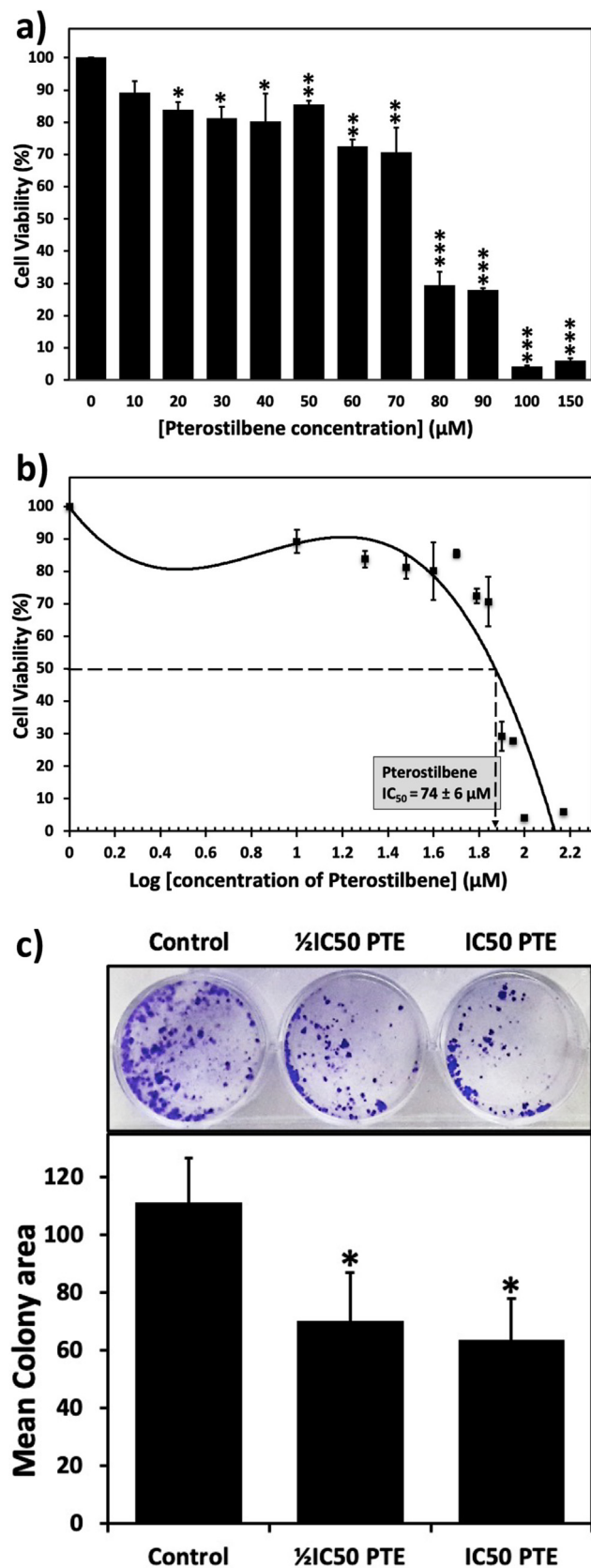
TEM (Fig. 5). The TEM revealed numerous evident filopodia around control untreated HepG2 cells which was markedly reduced after PTE treatments. Increased incidents of pyknotic nuclei, apoptotic bodies, cytoplasmic vacuolization, and accumulation of lipid droplets in the cytoplasm were detected after PTE treatments (Fig. 5 e-l). Enlarged mitochondria and dilation of the endoplasmic reticulum, in comparison to their sizes in the untreated control cells, were also detected (Fig. 5 h-l). IC_{50} of PTE induced fragmentation and dissolution of the cellular content of some cells. Completely lysed cell membranes and cellular fragments of some cells were detected (Fig. 5j). The results of the TEM showed that PTE-treated HepG2 cells exhibited characteristic features of apoptosis which is in agreement with LM observations.

The ultrastructural changes/observations of the untreated and PTE-treated HepG2 cells were evaluated. Table 1 illustrates the parameters that were investigated including, apoptotic bodies, pyknotic nuclei, mitotic figures, pleomorphic mitochondria, aggregated mitochondria, enlarged mitochondria, dilated endoplasmic reticulum, filopodia, vacuolated cytoplasm, and cellular junction.

3.5. PTE downregulates mTOR, S6K1, STAT3 and modulates p53 expression

HepG2 cells were treated with $\frac{1}{2}IC_{50}$, or IC_{50} of PTE. Immunoblot analysis showed that PTE treatment exhibited a highly significant downregulation of mTOR, S6K1, and STAT3 protein levels in a dose-dependent manner (Fig. 6). However, the IC_{50} of PTE resulted in the insignificant upregulation of the p53 protein level. While PTE modulated the expression level of the tumour suppressor protein p53, it reduced the expression levels of mTOR, S6K1, and STAT3 proteins.

4. Discussion

Cancers are caused mainly due to the failure in controlling the replication/DNA repair machinery of cells (Singh et al., 2019). Hepatocellular carcinoma (HCC) is an aggressive malignant tumor and registers high rates of lethality (Sung et al., 2021). In the present study, Pterostilbene (PTE), a dimethylated analogue of Resveratrol was used to investigate its effect on HepG2 cells. Resveratrol is a well-known antioxidant and anticancer phytochemical that has been used in cancer research (Choudhari et al., 2020). The hallmarks of cancer include uncontrolled proliferation, accompanied by a disturbance in the apoptosis machinery (Singh et al., 2019). The effect of PTE on the proliferation and viability of cancer cells has been previously challenged using various cancer cell lines (Gao et al., 2021). The MTT assay was employed to assess the effect of PTE treatments on the viability of HepG2 cells. Data revealed a highly significant decline in cell viability after exposing cells to PTE. PTE was reported to induce a significant decrease in the viability of SMMC-7721 hepatocellular carcinoma cells after treatment for 24 h with 50 μM PTE (Qian et al., 2017). The dose-dependent inhibition in HepG2 cell proliferation observed in the current study is in agreement with others. PTE decreased the cell viability of dif-

Fig. 1. PTE reduces cell viability and colony-forming potential of HepG2 cells. a) Dose-dependent inhibition of the viability of cancer cells by PTE treatment. HepG2 were either untreated or treated with the indicated concentrations of PTE for 48 hrs. **b)** PTE IC_{50} equals to 74 ± 6 μM as illustrated from the anti-log concentrations. **c)** PTE reduces the colony formation potential of HepG2 cells. Cells were treated with $\frac{1}{2}IC_{50}$ or IC_{50} of PTE for 48 hrs. After two weeks, PTE reduced the colony-forming potential of HepG2 cells. Colonies were stained in 2% crystal violet. ImageJ software was used to calculate the colony area. Values were compared with their respective controls and statistically evaluated. $^*p < 0.05$; $^{**}p < 0.01$; and $^{***}p < 0.005$ represent significance.
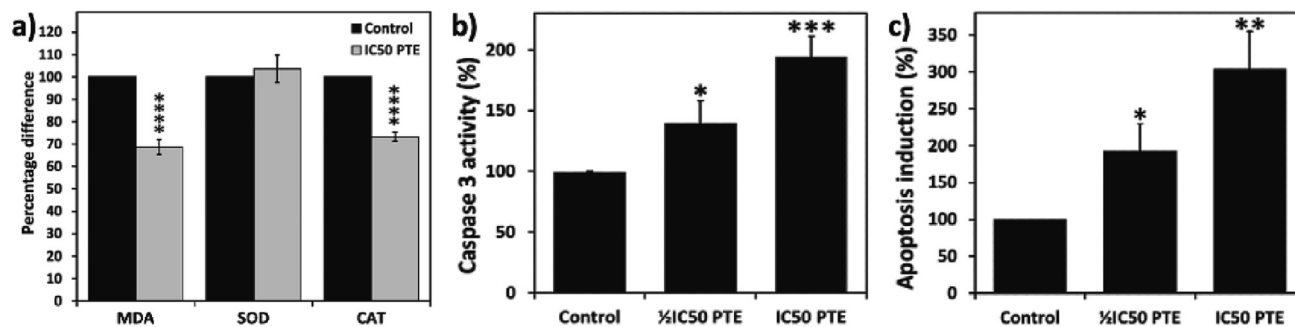
Fig. 2. PTE modulates oxidative stress and induces apoptosis in HepG2 cells. **a)** cells were treated with IC_{50} of PTE. PTE induced a significant reduction in malondialdehyde (MDA) and catalase (CAT) activity. However, the treatment with the IC_{50} PTE resulted in an insignificant increase in SOD activity. **b** and **c)** PTE induces apoptosis in HepG2 cells. PTE induced a significant increase caspase-3 activity (**b**) and histone release (**c**) in a dose-dependent manner. Values were compared with their respective controls and statistically evaluated. *$p < 0.05$; **$p < 0.01$; ***$p < 0.005$; and ****$p < 0.001$ represent significance.
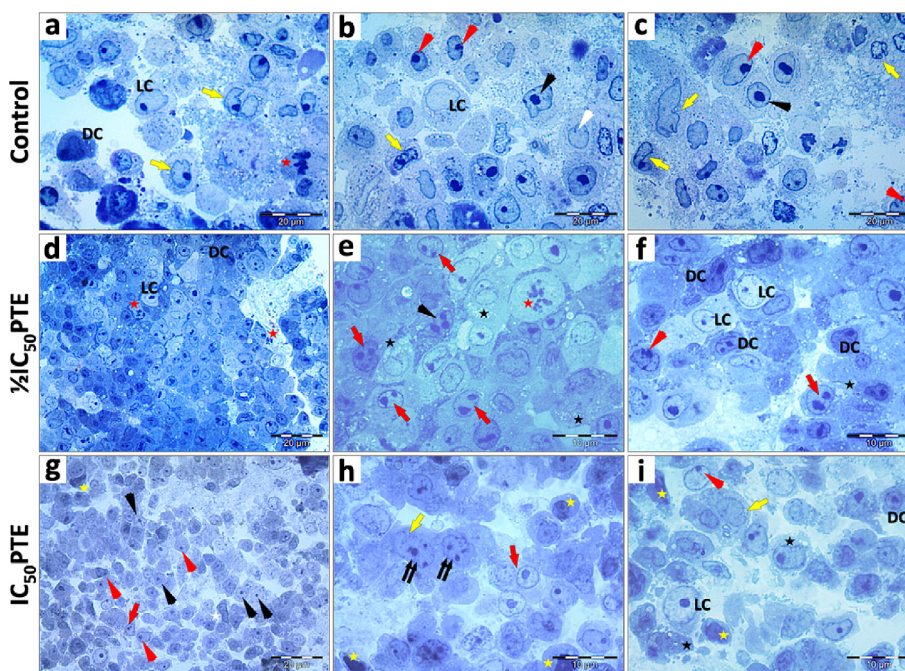
Fig. 3. Light micrograph (LM): Effect of PTE on HepG2 cells. a-c) Untreated HepG2 cells showing the morphological difference between light cells (LC) and dark cells (DC). Most cells are oval or round. DC exhibit densely stained cytoplasm, mitotic figures (red star), clefted nucleus (yellow arrow), peripheral nucleolus (red arrowhead), central nucleolus (black arrowhead) a small sized nucleus (white arrowhead). **d-f)** HepG2 cells treated with ½IC_{50} of PTE. **d)** The LM shows pleomorphic cells arranged in plates, pale LC, densely stained DC, mitotic figures (red star). **e)** The LM shows cells with a large nucleus, mitotic figure (red star), nuclei possessing double nucleoli (red arrow), or multiple nucleoli (black arrowhead), and cytoplasmic vacuolization (black star). **f)** The LM shows LC with large and rounded nuclei, DC with pleomorphic nuclei, cytoplasmic vacuolization (black star), some cells with peripheral nucleolus (red arrowhead), and double nucleoli in the nuclei (red arrow). **g-i)** HepG2 cells treated with IC_{50} of PTE. **g)** The LM shows cells with a pleomorphic shape, an increased incidence of centric nucleoli (black arrowhead), binucleated cells (red arrow), cells with irregular nuclei (white star), peripheral nucleoli (red arrowhead), and pyknotic nucleus (yellow star). **h)** The LM shows binucleated cells (red arrow), clefted nuclei (yellow arrow), multiple nucleoli (double arrows), and pyknotic nucleus (yellow star). **i)** The LM shows large LC with a large, rounded nucleus, DC nucleus with central nucleolus, and clefted nucleus (yellow arrow), peripheral nucleolus (red arrowhead), pyknotic nucleus (yellow star), and cytoplasmic vacuolization (black star). Specimens were fixed in $_4F_1G$ post-fixed in OsO_4 and stained with 1% Toluidine Blue. Magnification: d and g (x400) and a-c, e, f, h, and i (x1,000). Scale bar: a-d and g (20 μm) and e, f, h, and i (10 μm).

ferent multiple myeloma cells (Xie et al., 2016). Here, the IC_{50} for PTE against HepG2 cells was equal to 74 ± 6 μM. In addition, the clonogenic assay revealed that, upon PTE treatment, the potential of HepG2 cells to form colonies decreased. In agreement, PTE caused inhibition in the colony-forming ability of breast cancer cells (Daniel and Tollefsbol, 2018). The effect of PTE on other cancer cells have been previously assessed. In this context, in Molt-4 and Jurkat leukemic cell lines, PTE has showed an anti-cancer effect by elevating Fas expression level that resulted in apoptosis (Ramezani et al., 2019). Moreover, PTE exhibited an antiproliferation activity against C32 and A2058 Melanoma Cells (Wawszczyk et al., 2023). The antiproliferating capacity of PTE was further confirmed by examining HepG2 cells under light microscopy, which revealed a reduction in the number of mitotic figures after treatment with PTE, indicating a decrease in the dividing potential of cancer cells.

Redox equilibrium is crucial in all living organisms, and any disturbance in redox homeostasis as a result of the build-up of oxidizing molecules either by the overproduction or the diminished cellular reducing capacity may lead to the oxidation of biological molecules and, later, alter their physical properties, structure, and activity (Sharifi-Rad et al., 2020). The superoxide dismutase (SOD) enzyme catalyzes the conversion of superoxide radicals to H_2O_2 and oxygen, on the other hand, the catalase enzyme (CAT) detoxifies H_2O_2 into water and oxygen (Wang et al., 2018). In vitro approaches have showed that PTE possesses strong free radical scavenging/inhibiting activity (Acharya and Ghaskadbi, 2013).
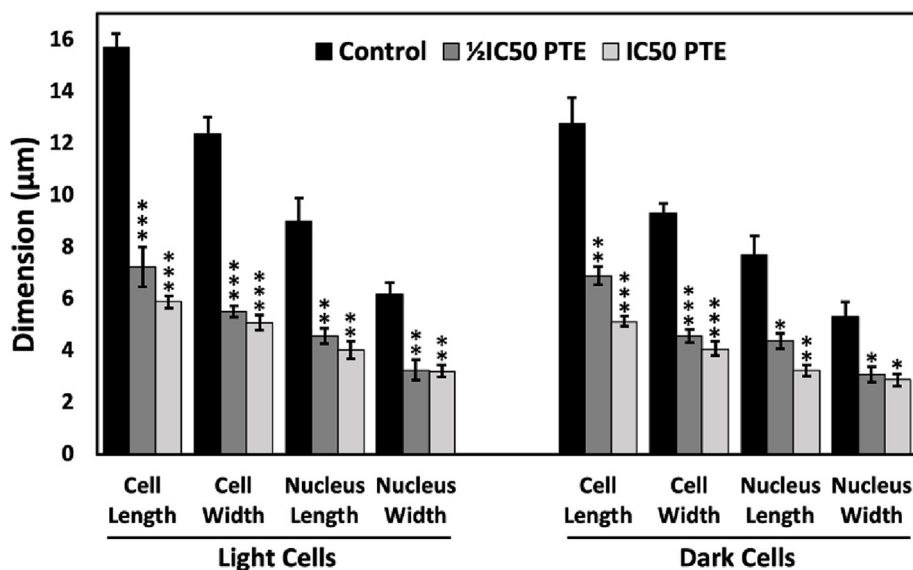
Fig. 4. Morphometric measurements of the light micrographs of PTE-treated HepG2 cells. Light and dark cells exhibited a significant decrease in cellular and nuclear dimensions after treatment with either ½IC$_{50}$ or IC$_{50}$ of PTE. ImageJ software was used for the morphometric measurements of HepG2 cells. Values were compared with their respective controls and statistically evaluated. *$p < 0.05$; **$p < 0.01$; and ***$p < 0.005$ represent significance.

Here, PTE-treated HepG2 cells exhibited insignificant increase in SOD activity and highly significant decrease in CAT activity. PTE treatment was shown to increase singlet oxygen and of H_2O_2 production, implying a ROS-induced apoptosis (Chakraborty et al., 2012). Furthermore, PTE-treated-MCF-7 treated with CAT exhibited a decrease in H_2O_2 levels accompanied by inhibition of PTE-induced cell death, confirming the involvement of H_2O_2 in PTE cytotoxicity (Chakraborty et al., 2010). HaCaT cells pre-treated with PTE and then co-treated with H_2O_2 had increased expression of SOD and glutathione but decreased catalase (Cheng et al., 2021). In addition, malondialdehyde (MDA) is an indicator for lipid peroxidation (Ayala et al., 2014). Here, PTE-treated cancer cells showed a highly significant decrease in MDA as reported previously (Pandey and Rizvi, 2011). Polyunsaturated fatty acids (PUFAs), which are targets of the lipid oxidation process, are converted to polyunsaturated fatty acyl-triacylglycerols and stored within lipid droplets during apoptosis (N. Li et al., 2018). This in turn will provide cells with protection from lipid-mediated toxicity and lipid peroxide-induced membrane damage during apoptosis and will decrease lipid peroxidation (N. Li et al., 2018). Studies showed that both ER stress and high levels of H_2O_2 induce the abundance of lipid droplets in HepG2 cells (Jin et al., 2018). Furthermore, increased levels of H_2O_2 may result in ER stress and apoptosis in other types of cancer (Pierre et al., 2014). Here, the increase in the activity of SOD, simultaneously with the decrease in CAT activity, may lead to an increase in H_2O_2 levels in PTE-treated HepG2 cells and may result in H_2O_2-induced apoptosis. Elevation in H_2O_2 levels along with ER stress led to the accumulation of lipid droplets, which helps to sequester polyunsaturated fatty acids, thus decreasing lipid peroxidation, which may mediate ferroptosis which is distinct from apoptotic cell death (Kajarabille and Latunde-Dada, 2019; N. Li et al., 2018).

It is well recognized that apoptosis has some characteristic features including; nuclear condensation, cellular shrinkage, oligonucleosomal DNA fragmentation, and nuclear fragmentations (Cavalcante et al., 2019; McIlwain et al., 2013). Caspases are endoproteases and important mediators of apoptosis. Many types of caspases function in the cell, including caspase 3, which is one of the most important caspases (Araya et al., 2021). Here, PTE-treated cancer cells exhibited a notable increase in the activity of caspase 3. Similarly, PTE induced caspases-8, −9, and −3 activation

(Xie et al., 2016). In apoptosis, oligo- and mononucleosomes are generated by inter-nucleosomal cleavage of chromatin which leads to DNA fragmentation (Gsell et al., 2020). Here, the percentage of DNA fragmentation, reflected by the amount of histone release, was elevated in PTE-treated HepG2 cells, which may indicate a possible apoptosis of HepG2 cells. As previously reported, PTE-treated melanoma cells (SK-MEL-2) exhibited DNA fragmentation and nucleosomal release (Huang et al., 2014). A well-known morphological apoptotic feature is apoptotic bodies, which are vesicles that are formed during the apoptotic process and contain fragments of dying cells. These bodies are then phagocytosed by macrophages and degraded (Gregory and Dransfield, 2018). EM showed increased incidence of apoptotic bodies in PTE-treated cells as reported previously in resveratrol-treated HeLa cells (L. Li et al., 2018).

Ultrastructural investigations revealed several PTE-induced morphological apoptotic features, including cell nuclear pyknosis. Pyknosis, an early apoptotic event, involves chromatin condensation and nuclear shrinkage (Hou et al., 2016; Prokhorova et al., 2018). Here, PTE-treated cancer cells exhibited a notable increase in the frequency of pyknotic nuclei. The incidence of pyknotic nuclei, as well as, fragmented DNA were reported in B16 melanoma cells treated with resveratrol (Gatouillat et al., 2010). Additionally, PTE treatment induced cellular fragmentation in HepG2 cells, which is a late apoptotic event of apoptosis (Wong, 2011). The TEM preparations showed few lipid droplets scattered in the cytoplasm of the control untreated HepG2 cells. Lipid droplets may be used by the cancer cells as a source of energy. A remarkable elevation in the incidence of lipid droplets were noticed in PTE-treated HepG2 cells. Lipid droplets are dynamic and are formed of a monolayer of phospholipids containing several proteins bounding neutral lipids that mainly consist of triacyl glycerides and cholesterol esters, which function in lipid metabolism and membrane trafficking (Olzmann and Carvalho, 2019). Cancer cells are often exposed to severe stress that weaken their ability to synthesize fatty acids. The survival of cancer cells depends on its ability to store lipids, as lipid droplets, from the microenvironment (Petan et al., 2018). Accumulation of lipid droplets in the cytoplasm may indicate apoptotic death (Boren and Brindle, 2012). Furthermore, vacuolization of the cytoplasm often accompanies different types of cell deaths, where in many cases irreversible vacuolization
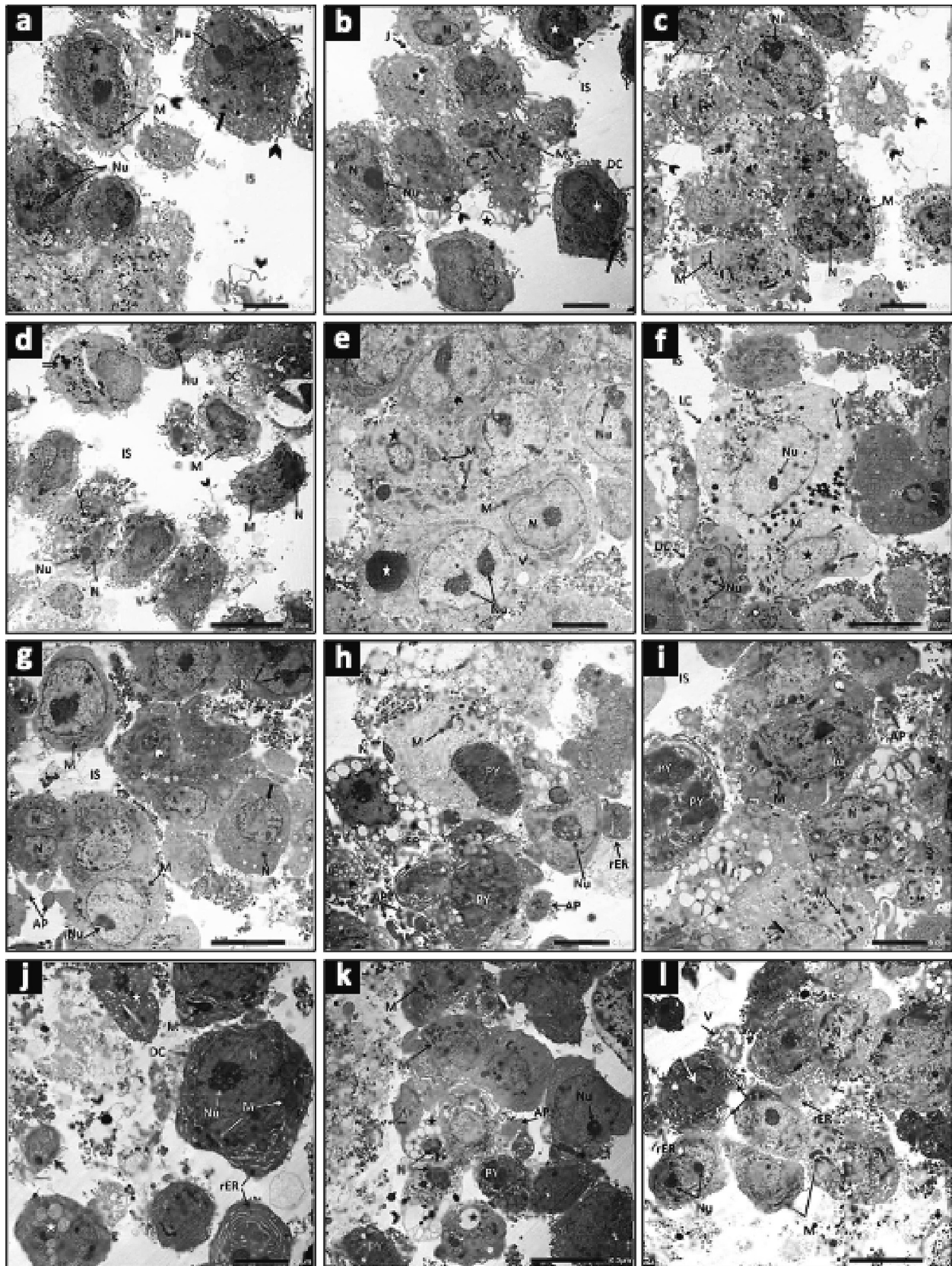
Fig. 5. Transmission electron micrograph (TEM): Effect of PTE on HepG2 cells. a-d) Control untreated HepG2 cells. **e-g)** HepG2 treated with ½IC$_{50}$. **h-l)** Cells treated with IC$_{50}$. TEM shows that PTE caused a reduction in the number of filopodia (arrowhead), accumulation of lipid droplets (L), enlargement in mitochondria (M), dilation of the endoplasmic reticulum (rER), formation of apoptotic bodies (AP), increased incidents of the pyknotic nucleus (Py), shrinkage nucleus (white arrow), shrunken cell (star), cell fragments with completely lysed cell membrane (double arrow) and furrow (triple arrow). Light cell (LC), dark cell (DC), intracellular space (IS), nucleus (N), nucleolus (Nu), vacuoles (v), cellular junctions (J), secretory granules (black arrow). Specimens were fixed in $_4F_1G$ post-fixed in OsO$_4$ and stained with uranyl acetate-lead citrate. Bar = 5 μm (a-c, e, and h-j); bar = 10 μm (d, f, g, k, and l).

Table 1

Scores of the ultrastructural observations of the untreated and PTE-treated HepG2 cells.

Ultrastructural observations	Untreated HepG2 cells	½IC$_{50}$ PTE	IC$_{50}$ PTE
Apoptotic body	–	+	+++
Pyknotic nuclei	–	+	+++
Mitotic figure	++	+	–
Pleoymorphic mitochondria	++	++	++
Agregated mitochondria	+	+	+
Enlarged mitochondria	–	+	++
Dilated endoplasmic reticulum	–	+	+++
Filopodia	+++	+	+
Vacuolated cytoplasm	+	+	++
Cellular junction	++	+	+

Cells were assessed on a scale from (–) to (+++) as follows: (–) = no change, (+) = mild change, (++) = moderate change, and (+++) = severe change.

is a hallmark of cytopathological conditions leading to cell death (Huang et al., 2020). After PTE treatment, the incidence of vacuolization of the cytoplasm was observed to increase in cells treated with PTE IC$_{50}$. In agreement, cytoplasmic vacuoles were detected in the bladder cancer cells (T24) treated with 100 μM of PTE (Chen et al., 2010).

Mitochondria regulate metabolism and other cellular function beside its crucial role in controlling apoptosis (Lee et al., 2022). Apoptosis is usually accompanied by mitochondrial swelling prior to other events including the disturbance in its membrane potential and the cytochrome *c* release into the cytosol (Elmore, 2007). Here PTE-treated cancer cells exhibited larger-sized and swollen mitochondria than those in the control untreated cells. Furthermore, the endoplasmic reticulum lumen of cancer cells treated with PTE IC$_{50}$ showed notable dilation and enlargement. These features have been reported previously in apoptotic cells (Bottone et al., 2013). The dilation of the endoplasmic reticulum lumen is an ultrastructure response to ER stress, an event that may contribute to apoptosis (Chavez-Valdez et al., 2016; Ozcan and Tabas, 2012).

The mTOR pathway is a crucial pathway that is abnormally regulated in many cancers (Zou et al., 2020). The mTOR kinase is related to the PIKK family of proteins (Feng et al., 2021). mTOR participates in the formation of two complexes, mTORC1 and mTORC2 (Ferrín et al., 2020; Khalil and Gout, 2012). Each mTOR complex has its physiological functions and downstream effector proteins.

mTORC1 functions in protein synthesis via S6K1 and 4E-BP proteins (Feng et al., 2021). mTORC1 activates S6K1 by phosphorylation, which in turn phosphorylates/activates different substrates that participate in the initiation of mRNA translation, including eIF4B (Ismail et al., 2014; Zou et al., 2020). Here, PTE treatment downregulated both mTOR and S6K1. In accordance, PTE significantly inhibited mTOR and S6K1 activation in primary spinal cord neurons (He et al., 2018).

Cell shrinkage, a characteristic feature of apoptosis, is manifested by cellular and nuclear shrinkage, denser cytoplasm, and tightly packed organelles (Banfalvi, 2016; Bortner and Cidlowski, 2020). Upon induction of apoptosis in HeLa S3, an apoptotic chromatin condensation occurs in three stages, the second of which is nucleus shrinkage (Toné et al., 2007). This occurs as apoptotic cells restructure their cytoskeleton to provide the plasticity required for cell volume reduction (Núñez et al., 2010). Here, morphometric measurements of LM preparations confirmed the significant shrinkage in the cellular and nuclear dimensions of PTE treated HepG2 cells. Interestingly, the downregulation of mTOR, which consequently lead to the downregulation of S6K1 upon treatment with PTE, may explain the notable shrinkage in the HepG2 cells (Fumarola et al., 2005). Cell shrinkage was observed after inhibition/deficiency of the S6K gene (Aguilar et al., 2007; Um et al., 2006). Relevantly, shrunken nuclei were observed in theca interstitial ovarian cells treated with resveratrol (Wong et al., 2010).

Metastasis in cancer requires the metastatic cells to go through severe steps including detachment, migration, invasion, and adhesion (Fares et al., 2020). Filopodia are finger-like cell protrusions formed of bundled actin that are crucial in cell–cell contacts, cell adhesion, migration, and angiogenesis (Arjonen et al., 2011; Gallop, 2020). The inhibition of the mTOR/S6K pathway results in the inhibition of cell motility and migration ability (Memmel et al., 2017). The inactivation of Raptor, a regulatory protein in mTORC1, was found to cause inhibition in the formation of filopodia (Solano and Odaka, 2019). The filopodia play key role in the migratory and invasive capacities of cancer cells (Jacquemet et al., 2015). Here, numerous filopodia were surrounding the untreated HepG2 cells as reported previously (Zhao et al., 2011). However, a considerable reduction in the filopodia was evident after treating cells with ½IC$_{50}$ of PTE. HepG2 treated with PTE IC$_{50}$ resulted in a smooth cell membrane without any protrusions which may imply the role of PTE in inhibiting the formation of filopodia. Thus, PTE may play a role in weakening the invasive abilities of HepG2 cells.
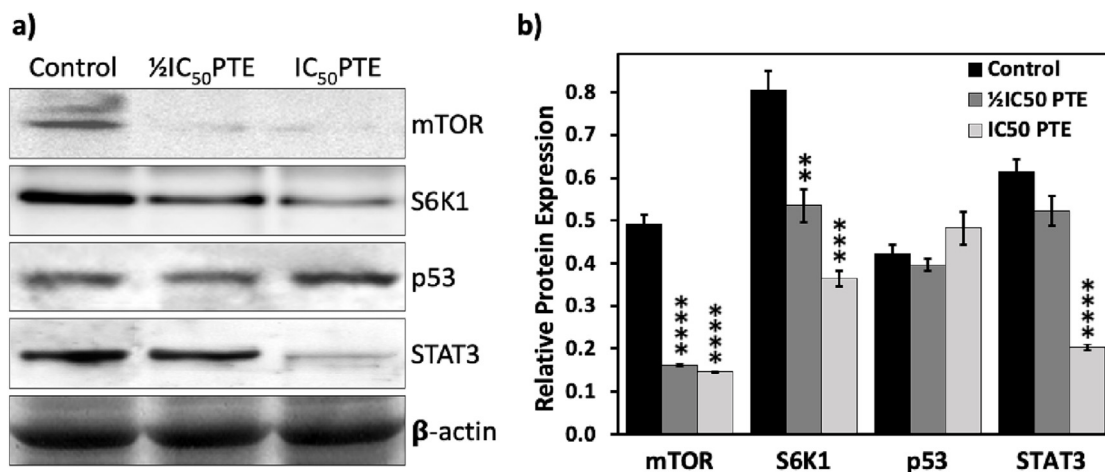
Fig. 6. PTE downregulates mTOR, S6K1, STAT3 and modulates p53. **a)** Cells were treated with ½IC$_{50}$ or IC$_{50}$ of PET for 48 hrs. **b)** Quantification of protein expression levels in HepG2 cells using Quantity One software. Values were compared with their respective controls and statistically evaluated. **$p < 0.01$; ***$p < 0.005$; and ****$p < 0.001$ represent significance.

P53, a transcription factor, activates numerous target genes involved in apoptosis induction (Hernández Borrero and El-Deiry, 2021). Here, the treatment with the IC_{50} of PTE modulated p53 expression in HepG2 as previously reported (Guo et al., 2016). PTE activated the wild type p53 in H460 lung cancer cells (Chen et al., 2017). It was reported that p53 upregulated SOD activity which may explain the increased levels of H_2O_2 and induction of H_2O_2-mediated apoptosis (Huang et al., 2020). Furthermore, p53 can bind to the prosurvival Bcl-2 protein family members, to release the proapoptotic proteins Bak and Bax, and induce mitochondrial apoptosis (Hernández Borrero and El-Deiry, 2021). p53 is involved in the ER-induced apoptosis via the activation of NOXA and PUMA located on the membranes of the ER (Hernández Borrero and El-Deiry, 2021). The p53-dependent accumulation of triacylglycerols containing polyunsaturated fatty acyl chains (PUFA-TAGs) during apoptosis was reported to occur via the activation of diacylglycerol acyltransferases (DGATs) (N. Li et al., 2018). Additionally, it has been reported that upregulated p53 induces the expression of its downstream target, p21, thereby inhibiting the G1/S transition in HepG2 cells and other models (Jiang et al., 2023; Karimian et al., 2016). Here, we did not assess the levels of p21 upon PTE treatments which is one of the limitations of the study.

Here, PTE negatively regulated the transcription factor STAT3 in HepG2 in a dose-dependent manner, as previously reported (Wen et al., 2018). Downregulation of STAT3 was correlated with modulation of p53 expression. It was previously reported that binding of STAT3 to the p53 promoter will provoke STAT3-induced inhibition of p53 (Niu et al., 2005). Blocking STAT3 upregulated p53 expression and induced p53-mediated apoptosis, an approach to reactivating p53 in many cancers (Niu et al., 2005). Additionally, the downregulation of STAT3 could be related to the modulation of p53, however, more research should be done to clarify the included mechanism (Pham et al., 2020). Investigating the levels of the activated form of STAT3 (pSTAT3), may clarify the mode of action. The downregulation of mTOR may explain the downregulation of STAT3. For its proper activity, STAT3 should be phosphorylated on Ser727 by mTOR (Rad et al., 2018). In addition, in response to stress signals, p53 activates PTEN, TSC2, and AMPK that negatively regulate mTOR (Cui et al., 2021).

5. Conclusions

The current results emphasise that PTE reduced the cell viability and colony-forming potential of the hepatocellular carcinoma HepG2 cells. The increase in histone release, increase in SOD activity, decrease in catalase activity and malondialdehyde, and the numerous lipid droplets in PTE-treated HepG2 may lead to apoptosis. PTE altered the morphology, reduced mitotic activity, and induced ultrastructural alterations in HepG2 cells. Additionally, PTE downregulated the expressions of mTOR, S6K1, STAT3, and modulated p53 expression. The data showed that the reduction in mTOR and S6K1 expressions may lead to several apoptotic features including notable cell shrinkage and a reduction in the number of filopodia of PTE treated HepG2 cells. Downregulated STAT3 correlated with the modulation of the expression level of the tumour suppressor protein p53 and positively affected the activity of caspase-3. The results of this study revealed that mTOR, S6K1, p53, and STAT3 may be involved in the anticancer mechanism of PTE against HepG2 cancer cells.

CRediT authorship contribution statement

Mahmoud I. Khalil: Conceptualization, Formal analysis, Supervision, Resources, Investigation, Methodology, Data curation, Writing – original draft, Validation, Writing – review & editing. **Alaa F. Agamy:** Methodology, Data curation, Writing – original draft. **Salma S. Elshewemi:** Methodology. **Ahmed S. Sultan:** Conceptualization, Formal analysis, Supervision, Resources, Investigation, Methodology. **Nabila E. Abdelmeguid:** Conceptualization, Formal analysis, Supervision, Methodology, Validation, Writing – review & editing.

Declaration of Competing Interest

The authors declare that they have no known competing financial interests or personal relationships that could have appeared to influence the work reported in this paper.

Appendix A. Supplementary material

Supplementary data to this article can be found online at https://doi.org/10.1016/j.sjbs.2023.103717.

References

Acharya, J.D., Ghaskadbi, S.S., 2013. Protective effect of Pterostilbene against free radical mediated oxidative damage. BMC Complement. Altern. Med. 13, 1–10. https://doi.org/10.1186/1472-6882-13-238.

Aguilar, V., Alliouachene, S., Sotiropoulos, A., Sobering, A., Athea, Y., Djouadi, F., Miraux, S., Thiaudière, E., Foretz, M., Viollet, B., Diolez, P., Bastin, J., Benit, P., Rustin, P., Carling, D., Sandri, M., Ventura-Clapier, R., Pende, M., 2007. S6 kinase deletion suppresses muscle growth adaptations to nutrient availability by activating AMP kinase. Cell Metab. 5, 476–487. https://doi.org/10.1016/j.cmet.2007.05.006.

Akinwumi, B.C., Bordun, K.-A.-M., Anderson, H.D., 2018. Biological activities of stilbenoids. Int. J. Mol. Sci. 19, 792. https://doi.org/10.3390/ijms19030792.

Araya, L.E., Soni, I. v, Hardy, J.A., Julien, O., 2021. Deorphanizing Caspase-3 and Caspase-9 Substrates In and Out of Apoptosis with Deep Substrate Profiling. ACS Chem Biol 16, 2280–2296. https://doi.org/10.1021/acschembio.1c00456

Arjonen, A., Kaukonen, R., Ivaska, J., 2011. Filopodia and adhesion in cancer cell motility. Cell Adh. Migr. 5, 421–430. https://doi.org/10.4161/cam.5.5.17723.

Ayala, A., Muñoz, M.F., Argüelles, S., 2014. Lipid peroxidation: production, metabolism, and signaling mechanisms of malondialdehyde and 4-hydroxy-2-nonenal. Oxid. Med. Cell Longev. 2014,. https://doi.org/10.1155/2014/360438 360438.

Banfalvi, G., 2016. Methods to detect apoptotic cell death. Apoptosis 22, 306–323. https://doi.org/10.1007/s10495-016-1333-3.

Boren, J., Brindle, K.M., 2012. Apoptosis-induced mitochondrial dysfunction causes cytoplasmic lipid droplet formation. Cell Death Differ. 19, 1561–1570. https://doi.org/10.1038/cdd.2012.34.

Bortner, C.D., Cidlowski, J.A., 2020. Ions, the movement of water and the apoptotic volume decrease. Front. Cell Dev. Biol. 8,. https://doi.org/10.3389/fcell.2020.611211 611211.

Bottone, M.G., Santin, G., Aredia, F., Bernocchi, G., Pellicciari, C., Scovassi, A.I., 2013. Morphological features of organelles during apoptosis: An overview. Cells 2, 294–305. https://doi.org/10.3390/cells2020294.

Cavalcante, G.C., Schaan, A.P., Cabral, G.F., Santana-da-Silva, M.N., Pinto, P., Vidal, A. F., Ribeiro-Dos-Santos, Â., 2019. A cell's fate: An overview of the molecular biology and genetics of apoptosis. Int. J. Mol. Sci. 20, 4133. https://doi.org/10.3390/ijms20174133.

Chakraborty, A., Gupta, N., Ghosh, K., Roy, P., 2010. In vitro evaluation of the cytotoxic, anti-proliferative and anti-oxidant properties of pterostilbene isolated from Pterocarpus marsupium. Toxicol. in Vitro 24, 1215–1228. https://doi.org/10.1016/j.tiv.2010.02.007.

Chakraborty, A., Bodipati, N., Demonacos, M.K., Peddinti, R., Ghosh, K., Roy, P., 2012. Long term induction by pterostilbene results in autophagy and cellular differentiation in MCF-7 cells via ROS dependent pathway. Mol. Cell Endocrinol. 355, 25–40. https://doi.org/10.1016/j.mce.2012.01.009.

Chavez-Valdez, R., Flock, D.L., Martin, L.J., Northington, F.J., 2016. Endoplasmic reticulum pathology and stress response in neurons precede programmed necrosis after neonatal hypoxia-ischemia. Int. J. Dev. Neurosci. 48, 58–70. https://doi.org/10.1016/j.ijdevneu.2015.11.007.

Checa, J., Aran, J.M., 2020. Reactive oxygen species: drivers of physiological and pathological processes. J. Inflamm. Res. 13, 1057–1073. https://doi.org/10.2147/JIR.S275595.

Chen, R.-J., Ho, C.-T., Wang, Y.-J., 2010. Pterostilbene induces autophagy and apoptosis in sensitive and chemoresistant human bladder cancer cells. Mol. Nutr. Food Res. 54, 1819–1832. https://doi.org/10.1002/mnfr.201000067.

Chen, R.-J., Wu, P.-H., Ho, C.-T., Way, T.-D., Pan, M.-H., Chen, H.-M., Ho, Y.-S., Wang, Y.-J., 2017. P53-dependent downregulation of hTERT protein expression and telomerase activity induces senescence in lung cancer cells as a result of pterostilbene treatment. Cell Death Dis. 8, e2985–e. https://doi.org/10.1038/cddis.2017.333.

Cheng, Y.-C., Chen, P.-Y., Way, T.-D., Cheng, C.-L., Huang, Y.-P., Hsia, T.-C., Chou, Y.-C., Peng, S.-F., 2021. Pre-Treatment of Pterostilbene Enhances H2O2-induced Cell Apoptosis Through Caspase-dependent Pathway in Human Keratinocyte Cells. In Vivo (Brooklyn) 35, 833–843. https://doi.org/https://doi.org/10.21873%2Finvivo.12324

Choudhari, A.S., Mandave, P.C., Deshpande, M., Ranjekar, P., Prakash, O., 2020. Phytochemicals in cancer treatment: from preclinical studies to clinical practice. Front. Pharmacol. 10, 1614. https://doi.org/10.3389/fphar.2019.01614.

Cui, D., Qu, R., Liu, D., Xiong, X., Liang, T., Zhao, Y., 2021. The cross talk between p53 and mTOR pathways in response to physiological and genotoxic stresses. Front. Cell Dev. Biol. 9,. https://doi.org/10.3389/fcell.2021.775507 775507.

Daniel, M., Tollefsbol, T.O., 2018. Pterostilbene downregulates hTERT at physiological concentrations in breast cancer cells: Potentially through the inhibition of cMyc. J. Cell Biochem. 119, 3326–3337. https://doi.org/10.1002/jcb.26495.

Elmore, S., 2007. Apoptosis: a review of programmed cell death. Toxicol. Pathol. 35, 495–516. https://doi.org/10.1080/01926230701320337.

Elsawy, H., Alzahrani, A.M., Alfwuaires, M., Sedky, A., El-Trass, E.E., Mahmoud, O., Abdel-Moneim, A.M., Khalil, M., 2021. Analysis of silymarin-modulating effects against acrylamide-induced cerebellar damage in male rats: Biochemical and pathological markers. J. Chem. Neuroanat. 115, 101964. https://doi.org/10.1016/j.biopha.2021.112180.

Elsherbini, A.M., Sheweita, S.A., Sultan, A.S., 2020. Pterostilbene as a phytochemical compound induces signaling pathways involved in the apoptosis and death of mutant P53-breast cancer cell lines. Nutr. Cancer 73, 1976–1984. https://doi.org/10.1080/01635581.2020.1817513.

Fares, J., Fares, M.Y., Khachfe, H.H., Salhab, H.A., Fares, Y., 2020. Molecular principles of metastasis: a hallmark of cancer revisited. Signal. Transduct. Target. Ther. 5, 28. https://doi.org/10.1038/s41392-020-0134-x.

Feng, Y., Chen, X., Cassady, K., Zou, Z., Yang, S., Wang, Z., Zhang, X., 2021. The role of mTOR inhibitors in hematologic disease: from bench to bedside. Front. Oncol. 10,. https://doi.org/10.3389/fonc.2020.611690 611690.

Ferrín, G., Guerrero, M., Amado, V., Rodríguez-Perálvarez, M., de la Mata, M., 2020. Activation of mTOR signaling pathway in hepatocellular carcinoma. Int. J. Mol. Sci. 21, 1266. https://doi.org/10.3390/ijms21041266.

Fumarola, C., la Monica, S., Guidotti, G., 2005. Amino acid signaling through the mammalian target of rapamycin (mTOR) pathway: Role of glutamine and of cell shrinkage. J. Cell Physiol. 204, 155–165. https://doi.org/10.1002/jcp.20272.

Gallop, J.L., 2020. Filopodia and their links with membrane traffic and cell adhesion. Semin. Cell Develop. Biol. 102, 81–89. https://doi.org/10.1016/j.semcdb.2019.11.017.

Gao, H., Liu, Z., Xu, W., Wang, Q., Zhang, C., Ding, Y., Nie, W., Lai, J., Chen, Y., Huang, H., 2021. Pterostilbene promotes mitochondrial apoptosis and inhibits proliferation in glioma cells. Sci. Rep. 11, 6381. https://doi.org/10.1038/s41598-021-85908-w.

Gatouillat, G., Balasse, E., Joseph-Pietras, D., Morjani, H., Madoulet, C., 2010. Resveratrol induces cell-cycle disruption and apoptosis in chemoresistant B16 melanoma. J. Cell Biochem. 110, 893–902. https://doi.org/10.1002/jcb.22601.

Gregory, C.D., Dransfield, I., 2018. Apoptotic tumor cell-derived extracellular vesicles as important regulators of the onco-regenerative niche. Front. Immunol. 9, 1111. https://doi.org/10.3389/fimmu.2018.01111.

Gsell, C., Richly, H., Coin, F., Naegeli, H., 2020. A chromatin scaffold for DNA damage recognition: how histone methyltransferases prime nucleosomes for repair of ultraviolet light-induced lesions. Nucleics Acids Res. 48, 1652–1668. https://doi.org/10.1093/nar/gkz1229.

Guo, L., Tan, K., Wang, H., Zhang, X., 2016. Pterostilbene inhibits hepatocellular carcinoma through p53/SOD2/ROS-mediated mitochondrial apoptosis. Oncol. Rep. 36, 3233–3240. https://doi.org/10.3892/or.2016.5151.

He, J.-L., Dong, X.-H., Li, Z.-H., Wang, X.-Y., Fu, Z.-A., Shen, N., 2018. Pterostilbene inhibits reactive oxygen species production and apoptosis in primary spinal cord neurons by activating autophagy via the mechanistic target of rapamycin signaling pathway. Mol. Med. Rep. 17, 4406–4414. https://doi.org/10.3892/mmr.2018.8412.

Hernández Borrero, L.J., El-Deiry, W.S., 2021. Tumor suppressor p53: Biology, signaling pathways, and therapeutic targeting. Biochim. Biophys. Acta Rev. Cancer 1876,. https://doi.org/10.1016/j.bbcan.2021.188556 188556.

Hou, L., Liu, K., Li, Y., Ma, S., Ji, X., Liu, L., 2016. Necrotic pyknosis is a morphologically and biochemically distinct event from apoptotic pyknosis. J. Cell Sci. https://doi.org/10.1242/jcs.184374.

Huang, B., Liu, J., Fu, S., Zhang, Y., Li, Y., He, D., Ran, X., Yan, X., Du, J., Meng, T., Gao, X., Liu, D., 2020. α-cyperone attenuates H(2)O(2)-induced oxidative stress and apoptosis in SH-SY5Y cells via activation of Nrf2. Front. Pharmacol. 11, 281. https://doi.org/10.3389/fphar.2020.00281.

Huang, X., Zhang, S.-Z., Wang, W.-X., 2014. Enhanced antitumor efficacy with combined administration of Astragalus and Pterostilbene for melanoma. Asian Pac. J. Cancer Prevent. 15, 1163–1169. https://doi.org/10.7314/apjcp.2014.15.3.1163.

Ismail, H.M.S., Hurd, P.J., Khalil, M.I.M., Kouzarides, T., Bannister, A., Gout, I., 2014. S6 kinase 2 is bound to chromatin-nuclear matrix cellular fractions and is able to phosphorylate histone H3 at threonine 45 in vitro and in vivo. J. Cell Biochem. 115, 1048–1062. https://doi.org/10.1002/jcb.24566.

Jacquemet, G., Hamidi, H., Ivaska, J., 2015. Filopodia in cell adhesion, 3D migration and cancer cell invasion. Curr. Opin. Cell Biol. 36, 23–31. https://doi.org/10.1016/j.ceb.2015.06.007.

Jiang, Y., Bi, J., Wu, M., Ye, S., Hu, L., Yi, Y., Wang, H., Wang, L., 2023. In vitro anti-hepatocellular carcinogenesis of 1, 2, 3, 4, 6-Penta-O-galloyl-β-D-glucose. Food Nutr Res 67. https://doi.org/10.29219%2Ffnr.v67.9244.

Jin, Y., Tan, Y., Chen, L., Liu, Y., Ren, Z., 2018. Reactive oxygen species induces lipid droplet accumulation in HepG2 cells by increasing Perilipin 2 expression. Int. J. Mol. Sci. 19, 3445. https://doi.org/10.3390/ijms19113445.

Kajarabille, N., Latunde-Dada, G.O., 2019. Programmed cell-death by ferroptosis: Antioxidants as mitigators. Int. J. Mol. Sci. 20, 4968. https://doi.org/10.3390/ijms20194968.

Karimian, A., Ahmadi, Y., Yousefi, B., 2016. Multiple functions of p21 in cell cycle, apoptosis and transcriptional regulation after DNA damage. DNA Repair (Amst.) 42, 63–71.

Khalil, M., Gout, I., 2012. Overexpression or downregulation of mTOR in mammalian cells. MTOR: Methods and Protocols 87–103.

Lee, Y.G., Park, D.H., Chae, Y.C., 2022. Role of mitochondrial stress response in cancer progression. Cells 11, 771. https://doi.org/10.3390/cells11050771.

Li, L., Qiu, R.-L., Lin, Y., Cai, Y., Bian, Y., Fan, Y., Gao, X.-J., 2018. Resveratrol suppresses human cervical carcinoma cell proliferation and elevates apoptosis via the mitochondrial and p53 signaling pathways. Oncol. Lett. 15, 9845–9851. https://doi.org/10.3892/ol.2018.8571.

Li, N., Sancak, Y., Frasor, J., Atilla-Gokcumen, G.E., 2018. A protective role for triacylglycerols during apoptosis. Biochemistry 57, 72–80. https://doi.org/10.1021/acs.biochem.7b00975.

McCormack, D., McFadden, D., 2013. A review of pterostilbene antioxidant activity and disease modification. Oxid. Med. Cell Longev. 2013,. https://doi.org/10.1155/2013/575482 575482.

McIlwain, D.R., Berger, T., Mak, T.W., 2013. Caspase functions in cell death and disease. Cold Spring Harb. Perspect. Biol. 5, a008656. https://doi.org/10.1101/cshperspect.a008656.

Memmel, S., Sisario, D., Zöller, C., Fiedler, V., Katzer, A., Heiden, R., Becker, N., Eing, L., Ferreira, F.L.R., Zimmermann, H., Sauer, M., Flentje, M., Sukhorukov, V.L., Djuzenova, C.S., 2017. Migration pattern, actin cytoskeleton organization and response to PI3K-, mTOR-, and Hsp90-inhibition of glioblastoma cells with different invasive capacities. Oncotarget 8, 45298–45310. https://doi.org/10.18632/oncotarget.16847.

Niu, G., Wright, K.L., Ma, Y., Wright, G.M., Huang, M., Irby, R., Briggs, J., Karras, J., Cress, W.D., Pardoll, D., Jove, R., Chen, J., Yu, H., 2005. Role of Stat3 in regulating p53 expression and function. Mol. Cell Biol. 25, 7432–7440. https://doi.org/10.1128/MCB.25.17.7432-7440.2005.

Núñez, R., Sancho-Martínez, S.M., Novoa, J.M.L., López-Hernández, F.J., 2010. Apoptotic volume decrease as a geometric determinant for cell dismantling into apoptotic bodies. Cell Death Differ. 17, 1665–1671. https://doi.org/10.1038/cdd.2010.96.

Olzmann, J.A., Carvalho, P., 2019. Dynamics and functions of lipid droplets. Nat. Rev. Mol. Cell Biol. 20, 137–155. https://doi.org/10.1038/s41580-018-0085-z.

Ozcan, L., Tabas, I., 2012. Role of endoplasmic reticulum stress in metabolic disease and other disorders. Annu. Rev. Med. 63, 317–328. https://doi.org/10.1146/annurev-med-043010-144749.

Pandey, K.B., Rizvi, S.I., 2011. Anti-oxidative action of resveratrol: Implications for human health. Arab. J. Chem. 4, 293–298. https://doi.org/10.1016/j.arabjc.2010.06.049.

Petan, T., Jarc, E., Jusović, M., 2018. Lipid droplets in cancer: Guardians of fat in a stressful world. Molecules 23, 1941. https://doi.org/10.3390/molecules23081941.

Petruzziello, A., 2018. Epidemiology of hepatitis B virus (HBV) and hepatitis C virus (HCV) related hepatocellular carcinoma. Open Virol. J. 12, 26–32. https://doi.org/10.2174/1874357901812010026.

Pham, T.-H., Park, H.-M., Kim, J., Hong, J.T., Yoon, D.-Y., 2020. STAT3 and p53: dual target for cancer therapy. Biomedicines 8, 637. https://doi.org/10.3390/biomedicines8120637.

Pierre, N., Barbé, C., Gilson, H., Deldicque, L., Raymackers, J.-M., Francaux, M., 2014. Activation of ER stress by hydrogen peroxide in C2C12 myotubes. Biochem. Biophys. Res. Commun. 450, 459–463. https://doi.org/10.1016/j.bbrc.2014.05.143.

Prokhorova, E.A., Kopeina, G.S., Lavrik, I.N., Zhivotovsky, B., 2018. Apoptosis regulation by subcellular relocation of caspases. Sci. Rep. 8, 12199. https://doi.org/10.1038/s41598-018-30652-x.

Qian, Y.-Y., Liu, Z.-S., Pan, D.-Y., Li, K., 2017. Tumoricidal activities of pterostilbene depend upon destabilizing the MTA1-NuRD complex and enhancing P53 acetylation in hepatocellular carcinoma. Exp. Ther. Med. 14, 3098–3104. https://doi.org/10.3892/etm.2017.4923.

Rad, E., Murray, J.T., Tee, A.R., 2018. Oncogenic signalling through mechanistic target of rapamycin (mTOR): A driver of metabolic transformation and cancer progression. Cancers (Basel) 10, 5. https://doi.org/10.3390/cancers10010005.

Ramezani, G., Pourgheysari, B., Shirzad, H., Sourani, Z., 2019. Pterostilbene increases Fas expression in T-lymphoblastic leukemia cell lines. Res. Pharm. Sci. 14, 55. https://doi.org/10.4103/1735-5362.251853.

Rashed, W.M., Kandeil, M.A.M., Mahmoud, M.O., Ezzat, S., 2020. Hepatocellular carcinoma (HCC) in Egypt: A comprehensive overview. J. Egypt. Natl. Canc. Inst. 32. https://doi.org/10.1186/s43046-020-0016-x.

Remsberg, C.M., Yáñez, J.A., Ohgami, Y., Vega-Villa, K.R., Rimando, A.M., Davies, N. M., 2008. Pharmacometrics of pterostilbene: preclinical pharmacokinetics and metabolism, anticancer, antiinflammatory, antioxidant and analgesic activity. Phytother. Res. 22, 169–179. https://doi.org/10.1002/ptr.2277.

Sharifi-Rad, M., Anil Kumar, N. v, Zucca, P., Varoni, E.M., Dini, L., Panzarini, E., Rajkovic, J., Tsouh Fokou, P.V., Azzini, E., Peluso, I., Prakash Mishra, A., Nigam, M., el Rayess, Y., Beyrouthy, M. el, Polito, L., Iriti, M., Martins, N., Martorell, M., Docea, A.O., Setzer, W.N., Calina, D., Cho, W.C., Sharifi-Rad, J., 2020. Lifestyle, Oxidative Stress, and Antioxidants: Back and Forth in the Pathophysiology of Chronic Diseases. Front Physiol 11, 694. https://doi.org/10.3389/fphys.2020.00694

Siegel, R.L., Miller, K.D., Jemal, A., 2020. Cancer statistics, 2020. CA Cancer J. Clin. 70, 7–30. https://doi.org/10.3322/caac.21590.

Singh, R., Letai, A., Sarosiek, K., 2019. Regulation of apoptosis in health and disease: the balancing act of BCL-2 family proteins. Nat. Rev. Mol. Cell Biol. 20, 175–193. https://doi.org/10.1038/s41580-018-0089-8.

Solano, A., Odaka, Y., 2019. Mechanism of filopodia formation in vascular endothelial cells. Undergraduate Scholarly Showcase.

Sung, H., Ferlay, J., Siegel, R.L., Laversanne, M., Soerjomataram, I., Jemal, A., Bray, F., 2021. Global cancer statistics 2020: GLOBOCAN estimates of incidence and mortality worldwide for 36 cancers in 185 countries. CA Cancer J. Clin. 71, 209–249.

Suzuki, H., Suzuki, K., 1998. Rat hypoplastic kidney (hpk/hpk) induces renal anemia, hyperparathyroidism, and osteodystrophy at the end stage of renal failure. J. Vet. Med. Sci. 60, 1051–1058. https://doi.org/10.1292/jvms.60.1051.

Tahtamouni, L., Ahram, M., Koblinski, J., Rolfo, C., 2019. Molecular regulation of cancer cell migration, invasion, and metastasis. Anal. Cell Pathol. (Amst.) 2019, 1356508. https://doi.org/10.1155/2019/1356508.

Toné, S., Sugimoto, K., Tanda, K., Suda, T., Uehira, K., Kanouchi, H., Samejima, K., Minatogawa, Y., Earnshaw, W.C., 2007. Three distinct stages of apoptotic nuclear condensation revealed by time-lapse imaging, biochemical and electron microscopy analysis of cell-free apoptosis. Exp. Cell Res. 313, 3635–3644. https://doi.org/10.1016/j.yexcr.2007.06.018.

Um, S.H., D'Alessio, D., Thomas, G., 2006. Nutrient overload, insulin resistance, and ribosomal protein S6 kinase 1, S6K1. Cell Metab. 3, 393–402. https://doi.org/10.1016/j.cmet.2006.05.003.

Wang, Y., Branicky, R., Noë, A., Hekimi, S., 2018. Superoxide dismutases: Dual roles in controlling ROS damage and regulating ROS signaling. J. Cell Biol. 217, 1915–1928. https://doi.org/10.1083/jcb.201708007.

Wawszczyk, J., Jesse, K., Kapral, M., 2023. Pterostilbene-mediated inhibition of cell proliferation and cell death induction in amelanotic and melanotic melanoma. Int. J. Mol. Sci. 24, 1115. https://doi.org/10.3390/ijms24021115.

Wen, W., Lowe, G., Roberts, C.M., Finlay, J., Han, E.S., Glackin, C.A., Dellinger, T.H., 2018. Pterostilbene suppresses ovarian cancer growth via induction of apoptosis and blockade of cell cycle progression involving inhibition of the STAT3 pathway. Int. J. Mol. Sci. 19, 1983. https://doi.org/10.3390/ijms19071983.

Wong, R.S.Y., 2011. Apoptosis in cancer: from pathogenesis to treatment. J. Exp. Clin. Cancer Res. 30, 87. https://doi.org/10.1186/1756-9966-30-87.

Wong, D.H., Villanueva, J.A., Cress, A.B., Duleba, A.J., 2010. Effects of resveratrol on proliferation and apoptosis in rat ovarian theca-interstitial cells. Mol. Hum. Reprod. 16, 251–259. https://doi.org/10.1093/molehr/gaq002.

Xie, B., Xu, Z., Hu, L., Chen, G., Wei, R., Yang, G., Li, B., Chang, G., Sun, X., Wu, H., Zhang, Y., Dai, B., Tao, Y., Shi, J., Zhu, W., 2016. Pterostilbene inhibits human multiple myeloma cells via ERK1/2 and JNK pathway in vitro and in vivo. Int. J. Mol. Sci. 17, 1927. https://doi.org/10.3390/ijms17111927.

Zhao, R., Wang, T.-Z., Kong, D., Zhang, L., Meng, H.-X., Jiang, Y., Wu, Y.-Q., Yu, Z.-X., Jin, X.-M., 2011. Hepatoma cell line HepG2.2.15 demonstrates distinct biological features compared with parental HepG2. World J. Gastroenterol. 17, 1152–1159. https://doi.org/10.3748/wjg.v17.i9.1152.

Zhu, Y., Li, M., Wang, X., Jin, H., Liu, S., Xu, J., Chen, Q., 2012. Caspase cleavage of cytochrome c1 disrupts mitochondrial function and enhances cytochrome c release. Cell Res. 22, 127–141. https://doi.org/10.1038/cr.2011.82.

Zou, Z., Tao, T., Li, H., Zhu, X., 2020. mTOR signaling pathway and mTOR inhibitors in cancer: progress and challenges. Cell Biosci. 10, 31. https://doi.org/10.1186/s13578-020-00396-1.